Proceedings of 2018 IEEE
International Conference on Mechatronics and Automation
August 5 - 8, Changchun, China

Hydrodynamic Analysis of a Novel Thruster for Amphibious Sphere Robots

Xihuan Hou[1,2] , Shuxiang Guo[1,2,3]*, Liwei Shi[1,2]*, Huiming Xing[1,2], Shuxiang Su[1,2], Zhan Chen[1,2]
Yu Liu[1,2], Huikang Liu[1,2]

[1]*Key Laboratory of Convergence Medical Engineering System and Healthcare Technology, The ministry of Industry and Information Technology, Beijing Institute of Technology*
No.5, Zhongguancun South Street, Haidian District, Beijing 100081, China
[2]*Key Laboratory of Biomimetic Robots and Systems, Ministry of Education, Beijing Institute of Technology*
No.5, Zhongguancun South Street, Haidian District, Beijing 100081, China
[3]*Faculty of Engineering, Kagawa University, 2217-20 Hayashi-cho, Takamatsu, Kagawa, Japan*
shiliwei@bit.edu.cn, 3120170428@bit.edu.cn, guoshuxiang@bit.edu.cn
**Corresponding author*

***Abstract* – Four novel thrusters as the actuator of amphibious spherical robots play an important role. The resultant force of four thrusters is the main driving force of the robot. In order to achieve better control of the amphibious spherical robots, it is necessary to analyze the effects on the propelling force of the novel thruster. This paper utilize Computational Fluid Dynamics (CFD) to simulate hydrodynamic behavior of the new thruster and analyze the thrust force with different rotating velocity and inlet velocity. Further, as the inlet velocity is susceptible by the rotating velocity, we defined advanced coefficient with inlet velocity and rotating velocity. We analyze the thrust force and efficiency with different advanced coefficients. The result shows that the thrust force is more sensitive to rotating velocity of blades than the inlet velocity. The curves also show that the efficiency traces a downward parabola with the advanced coefficient. According to the simulation results, I should keep the advanced coefficient at 0.6 as our best as possible to take full use of the energy. Thus, these results provide foundation for the mathematical model building.**

Index Terms – Amphibious sphere robot, Water-jet thruster, computational fluid dynamics (CFD), thrust force.

I. INTRODUCTION

Inspired by some amphibious animals which can move on land and in water and even on the water bottom, a kind of amphibious sphere robots have been the focus of many researchers [1]. They were developed for many applications which benefit from the ability of amphibious movement and the zero turning radius including pollution detection terrain mapping, and scouting potential approach lanes for amphibious naval operation in narrow areas[2]. The actuating structure of amphibious sphere robots plays a vital role for the motion in turbulent zones covering lands, underwater and transition regions. With the development of amphibious sphere robots, many kinds of driving appliances have appeared. Different application fields adopt different propulsion methods.

In 2006, inspired by vertebrates, Alessandro Crespi et al. designed an amphibious snake robot called AmphiBot II [3] controlled by on-board central pattern generator (CPG). In 2013, Alessandro Crespi designed a bio-amphibious salamander robot called Salamandra robotica II [4] with four legs walking on the ground based on various gaits by the body-limb coordination and body undulation，and an actuated spine swimming in water. Xie G designed a salamander-like robot called Chigon[5] which owned a novel mechanical structure containing four limps and a multiple segments linked tail. In 2012, a versatile amphibious robot, AmphiRobot-II [6], was designed by Junzhi Yu. The robot equipped with a novel hybrid propulsive mechanism coupled with wheel-propeller-fin movements. The robot is not only able to implement flexible wheel-based movements on land, but also to perform steady and efficient fish- or dolphin-like swimming under water and also can further switch between these two patterns via a specialized swivel device.

The above four amphibious robots have the same characteristics, snake-like and multi-link. Most own composite actuators. They move by crawling or wheel on land and by fins or swing of the body in the water. Later, for simplify the structure, a kind of amphibious robots is equipped with a component as the actuated structure of land and underwater. In 2009, a wheel-propeller-leg integrated amphibious robot [7] was developed by Yuangui TANG. The robot integrated the common mobile mode of the underwater robot, propeller and the robot on land, wheel-leg. In 2016, Shiwu Zhang developed an amphibious robot AmphiHex-I propelled by six specially designed transformable curved flipper legs [8]. The robot can walk on rough terrains, maneuvering underwater, and pass through soft muddy or sandy substrates in the littoral area between land and water. When the robot swims in the water, the legs propel the robot like paddles.

All of above robots almost show elongated shape limiting them to work in broad areas. The driving appliances of above robots, fin or propeller, tend to break down because of abrasion and twining of weeds. To solve these problems, our teams developed two amphibious quadruped spherical robots (ASR-I) and ASR-II [9,15]. The propulsion device of ASR is a cylinder duct thruster, just as shown in Fig.1 [16-19]. When the robot walks on land, the motor of the cylinder thruster does not work and the thruster was just as a leg. When the robot moves in the water, the thruster inhales water from the inlet based on the working propeller then jets water from the nozzle to propel the robot. While there are two disadvantages of this thruster. First,

the thrust force of the propeller is too small to propel the robot. Second, the outlet of the thruster is too narrow to keep the robot walking steadily on land.

In order to overcome above defects, our team proposed a new water-jet thruster. The new duct thruster is improved mainly at two aspects. First, duct of the novel thruster owns larger diameter and is made of aluminium alloy, which can improve the stability when the robot standing on land; Second, the nozzle of the thrust is cone, which can generate stronger force.

Fig. 1 The water-jet thruster in previous work.

In order to make use of the new thruster to control amphibious spherical robots with four new thrusters, it is necessary to investigate the thrust force of the new thruster. With the rapid development of computer technology and Computational Fluid Dynamic (CFD), the hydrodynamic analysis have been widely applied to analysis the characters of water-jet thruster or propeller. In this article, I investigated the hydrodynamic performance of the new thruster with CFX software.

The rest of this paper is organized as follows. Section II depicts the amphibious sphere robot and the prototype of the novel water-jet thruster. The hydrodynamic simulation process and results are shown in Section III. Finally, Section IV concludes this paper with an outline of future work.

II. THE NOVEL WATER-JET THRUSTER

A. The Prototype of Novel Thruster

The propulsion system composed of four vector water-jet thruster is the crucial factor of the Amphibious Sphere Robot as shown in Fig.2 (a). Because it is the lowest layer in the control loop of the system. In previous researches, the thrust force of the propulsion system is too small to drive the robot in the water. In this paper, I designed a new thruster just as shown in Fig.2 (b). Fig.3 gives the different viewports of the 3D model of the new thruster. The novel thruster mainly consists of four parts, motor, propeller, inlet dam-board and nozzle. The propeller owns five blades surrounded by a long duct, which can protect from abrasion and wind. The nozzle of the thruster shows cone, which can make larger thruster force than cylinder. Concrete geometric parameters of the new thruster are listed in Fig.4 and Table 1.

B. Simplified Model of the thruster for hydrodynamic analysis

Because there exist some parts in the physical model no effects on hydrodynamic simulation. It is necessary to simplify the 3D model for CFD simulation. It can get effective results and reduce the computational time. The omitted parts are listed as following.

1. The motor of thruster has complicated structure. Outline of the motor is cylinder. The motor can be simplified a cylinder.
2. The duct of the thruster can be simplified as a cylinder omitting some irregular solids.
3. Some parts such as screw and nuts have been omitted. The simplified model is shown in Fig.5.

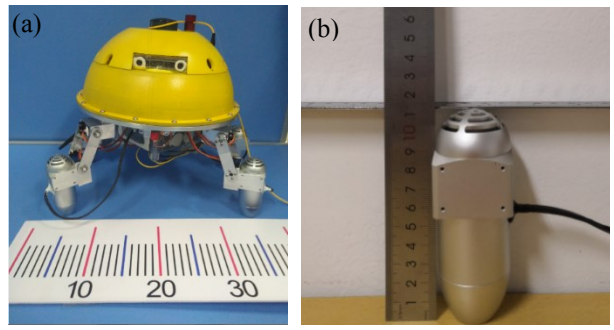

Fig.2 Prototype of amphibious sphere robot and new thruster. (a) Prototype of amphibious sphere robot. (b) Prototype of new thruster.

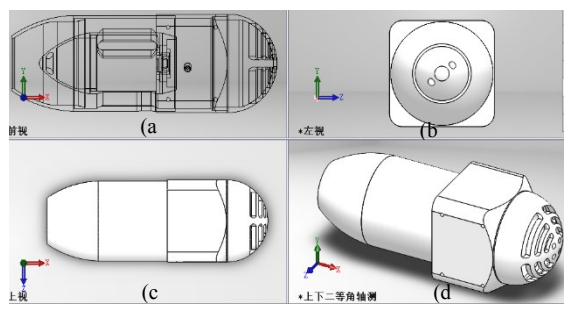

Fig.3 Different views of the thruster. (a) Front viewport of the thruster. (b) Left viewport of the thruster. (c) Top viewport of the thruster. (d) Axonometric viewport of the thruster

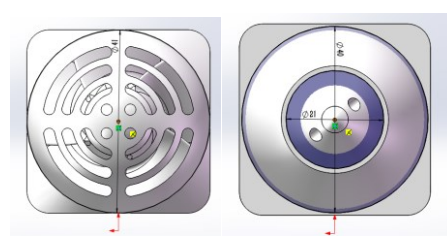

(a) Diameter of dam-board (b) Diameter of dam-board

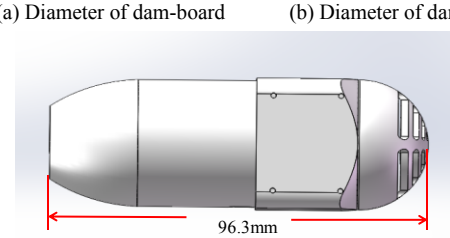

(c) Length of thruster

Fig.4 Size of the new thruster

TABLE I
THRUSTER GEOMETRIC PARAMETERS

Parameter	Value
Propeller Diameter	D=36.5mm
Number of blades	Z=5
Thruster length	L=96.3mm
Nozzle Diameter	21mm
Rated power of motor	80W

III. HYDRODYNAMIC ANALYSIS OF THE NOVEL THRUSTER

Hydrodynamic simulation can exhibit the flow phenomenon clearly of the inner and surrounding of the thruster[20]. It is convenient to observe if there exist backflow, cavitation and so on, which can provide some bases for the optimization of the thruster. Then several vital hydrodynamic parameters which influence the thruster force were analyzed which can control the thruster force in the water efficiently. In the following research, all the simulations were calculated by CFX which is associated with ANSYS WORKBENCH.

A. Mesh Generation and Boundary Conditions

After modeling the novel thruster, we need established the computation domain. The computational domain affects the hydrodynamic characteristic of the thruster, so it should be large enough to ensure that the wall of the computational domain cannot affect the hydrodynamic results and be long enough to observe the wake from the nozzle [21]. The computational domain consists an internal rotating cylinder containing the propeller of the thruster and an external stationary cylinder with radius 5D and with length 10L. The thruster was put in the center of the computation domain. Fig.6 shows the computational domain.

The mesh of all domains is also a key factor of hydrodynamic analysis. In this research, the mesh operation was performed using ANSYS Workbench CFX Mesh. Because the quality and amount of the mesh determine the reliability of results and efficiency of the simulation correspondingly, we should set different size of the mesh aiming at obtaining proper grid. All domains were dived into two sections [22]:

1. Stationary domain with larger mesh;
2. Rotating domain around propeller with small mesh as shown in Fig.7.

According to the influence to the hydrodynamic characteristic, some areas needs set size along to refine, such as the propeller and areas around the thruster. Fig.8 shows the various meshed section which are merged for CFD analysis by the mesh generator. The total number of the elements was 2,186,476, and the total number of nodes was 684,221.

Then, the boundary conditions of all domains were necessary before starting solver. In this research, boundaries make up of velocity inlet and pressure opening. Because the flow out of the nozzle have no fixed direction in the real environment, the walls except the inlet were set as opening boundary. In this hydrodynamic model, the gravity and buoyancy were both ignored. The environment condition is set as the isothermal temperature of 20 ℃. In this analysis, the rotational velocity of the propeller was imposed by a Moving Reference Frame (MRF) applied to inner region of the domain due to low time in computation and acceptable accuracy in simulation [23]. Fig.9 shows the boundary of all domains.

B. Solver Settings

The RANS (Reynolds Averaging Navier-Stokes) equations are solved numerically by a finite volume technique. Also, high resolution method was used to discrete equations and first order method was applied to investigate turbulence [22]. Moreover, in order to choose correct fluid model, we calculated the Reynolds number R_e , $R_e = \frac{\rho v d}{\mu}$ [21].Where, ρ is the density of the fluid, v is the relative velocity of the thruster to the fluid, the maximum to $0.6\,m/s$. d is the diameter of the thruster as 0.04 m , μ is the viscosity coefficient, which is 1×10^{-6} at 20℃. So the Reynolds number is $R_e = 2.4\times10^{-5}$, which indicates that the flow is turbulent when the thruster is working. Then, Shear Stress Transport (SST) turbulence model was selected since it was applied in most researches due to its higher accuracy. The convergence criterion adopt the average residuals based on all controls RMS (Root Mean Square) and amount was set as 1×10^{-5} in the solver control. For accuracy in solver results, a user monitor about the flow velocity of a point at the nozzle was used to guarantee the convergence.

C. Simulation Results

From theoretical analysis, the thrust force is mainly affected the inlet velocity, the rotational velocity of the motor. In order to analysis factors effects on the thrust force, we must set relative boundary conditions to process the hydrodynamic simulation.

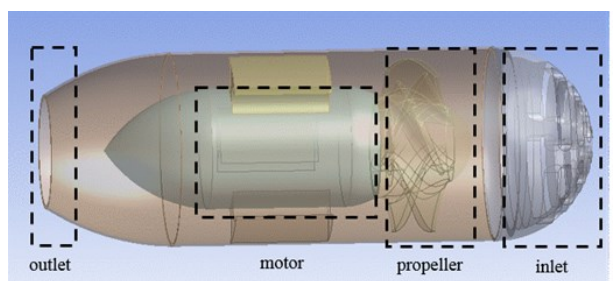

Fig.5 Simplified 3D model of the thruster

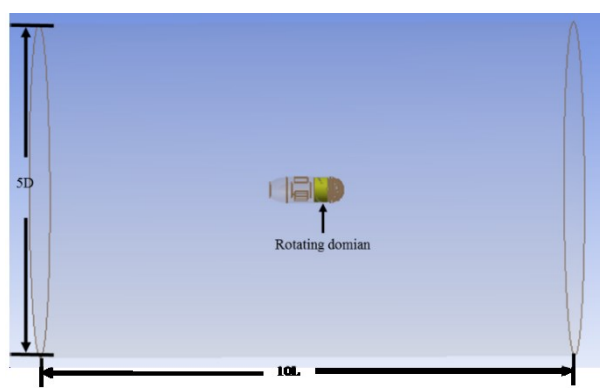

Fig.6 Global view of the computational domain

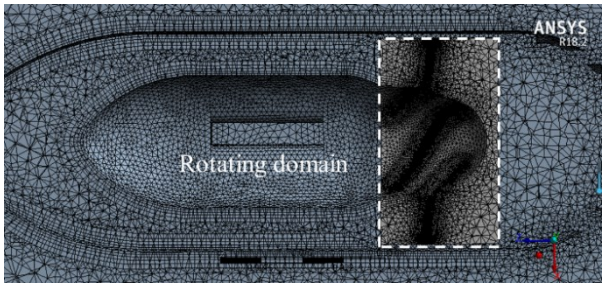

Fig.7 Division of calculation domain with mesh

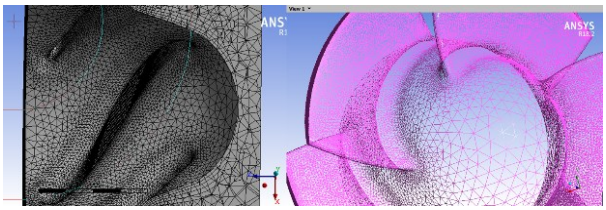

Fig.8 Mesh cells on the propeller at different views

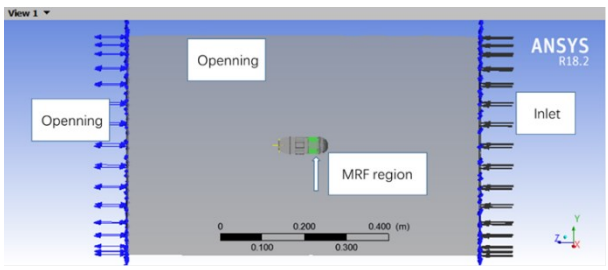

Fig.9 Boundary conditions of all domains

First, we analyzed the effects of the rotating velocity on the thrust force. We processed the hydrodynamic simulation with rotating velocity varying from 1000rpm to 7000rpm and constant inlet velocity, as 0.1m/s. In addition, the reference pressure of all domains is 1atm. In the practical experiment, the thruster was placed at the depth of 1m, so the relative pressure of the opening was set as 0.098atm. In all simulations the sets of the pressure kept unchanged. To save space, the following only show partial contour maps of the velocity and pressure. Fig.10 (a) shows the velocity vary of the water in and around the thruster, and different colours represent different velocity value. Fig.10 (b) shows the distribution of the velocity at the nozzle. The flow is accelerated through the blades up to a maximum velocity of **0.7m/s** at the nozzle which is **7 times** of the inlet velocity, and average velocity of the nozzle plane reaches **0.58m/s**. Just as shown in Fig.10 (c), the velocity from the edge of the blade to the root gradually declines. Fig.11 shows contour maps of the pressure. The pressure around the blade and at the nozzle is lower than other points. To observe the distribution of velocity and pressure, the phenomenon is apparent, which is a point with high velocity and low pressure. Maybe this phenomenon corresponds the Bernoulli equation. The velocity goes up gradually from the root to the edge on the blade just as shown in Fig.12. Fig.13 shows the pressure distribution on the two plane of the blade. The pressure declines sharply at the back of the blade， recoveries and increases constantly. Thus, there exists a difference in pressure， which generates a thrust force with the opposite direction of the incoming flow [24].

The contours maps of velocity and pressure just reflect the changes of the flow in the thruster. While, the concrete changes of the thrust force inflected by inlet velocity and rotating velocity will be shown in the following. Since the thrust force is along the negative Z axis, the value is negative. Fig.15 shows that the thrust force gradually gets larger as the rotating velocity rising. When the rotating velocity below 2000rpm, the gradient of thrust ascent is relative small. Because at this situation the brushless DC motor in the thruster is unstable and low efficiency. Just as shown in Fig.15, the thrust force enlarges fast in a more liner fashion, when the rotating velocity higher than 3000rpm.

Then, the effects of the inlet velocity on the thrust force were investigated. We processed the hydrodynamic simulation with inlet velocity varying from 0m/s to 0.7 m/s and a constant rotating velocity, as 3500rpm, 4500rpm, 5500rpm and 6500rpm. Fig.16 depicts the thrust force changing at different flow inlet velocity. On the whole, the influence of flow inlet velocity on the thrust force is slight, especially at a low rotating velocity.

In fact, the inlet velocity which may be the velocity of fluid or the advance speed of the ASR with four novel thrusters changes with the rotating velocity. Generally, thrust coefficient, torque coefficient and efficiency of propellers change with advanced coefficient are analyzed. In this section, we will reveal the characteristic curve of the novel thruster about these parameters. These parameters are defined as follows:

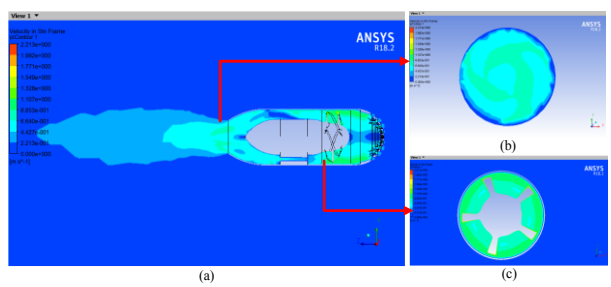

(a) (b) (c)

Fig.10 Contours of velocity at 0.1 m/s and 1000rpm

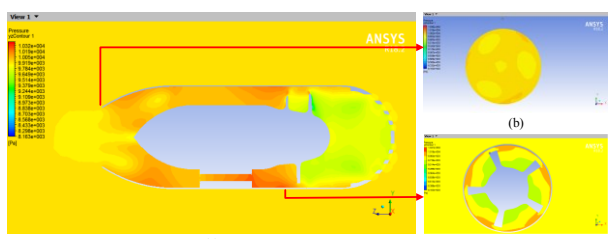

(a) (b) (c)

Fig.11 Contours of pressure at 0.1 m/s and 1000rpm

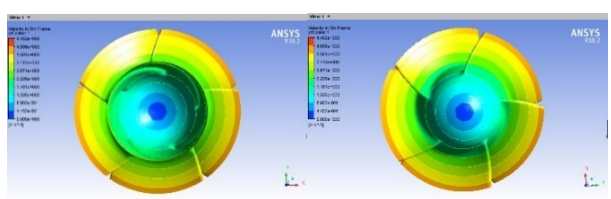

(a) Inlet plane (b) Outlet plane

Fig.12 Velocity distribution on blade

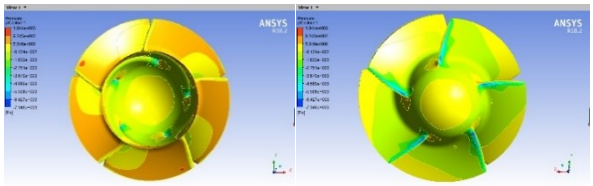

(a) Inlet plane (b) Outlet plane

Fig.13 Pressure distribution on blade

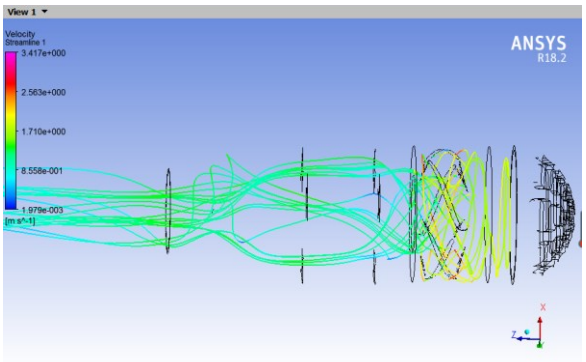

Fig.14 Streamline of the flow in the thruster

$$J=\frac{V}{nD},\qquad K_T=\frac{T}{\rho n^2 D^4}$$

$$K_Q=\frac{Q}{\rho n^2 D^5},\qquad \eta=\frac{K_T}{K_Q}\cdot\frac{J}{2\pi}$$

In the simulation, the advanced coefficient J was set in the range from 0 to 0.3, and the rotating velocity of the blade was set as a constant value 500r/s. We controlled the changes of the advanced coefficient by the inlet velocity. Changes of the thrust coefficient and torque coefficient with the advanced coefficients are shown in Fig.17. Fig.18 shows the thrust force with different advanced coefficients. According to Fig.17, the efficiency rise a maximum at $J=0.55$. In Fig.18, the thrust force decreases with the advanced coefficient. When the robot starts, we can adopt a smaller advanced coefficient to get larger force. When the robot runs, we can adopt a larger advanced coefficient to get larger efficiency.

IV. Conclusion

This paper adopted the CFX module of software Ansys18.0 to analysis the thrust force of a new water-jet thruster. Both The rotating velocity and the inlet velocity have effects on thrust force. Relationship between the efficiency and advanced coefficient shows that the efficiency get maximum at $J=0.55$. According to these results, we can adjust rotating velocity of every thruster to change the resultant force of the robot, and keep the robot moving with an expected posture. When the energy is limiting, we can keep all thrusters at $J=0.55$ to make full use of the energy according to the result.

In the future, we need to verify the accuracy of the hydrodynamic simulation through experiments. In order to control the robot, it is necessary to build the mathematical model of the new thruster based on the simulation data. We can get the thrust force of every thruster based on the mathematical model, which can provide foundation for the design of controller.

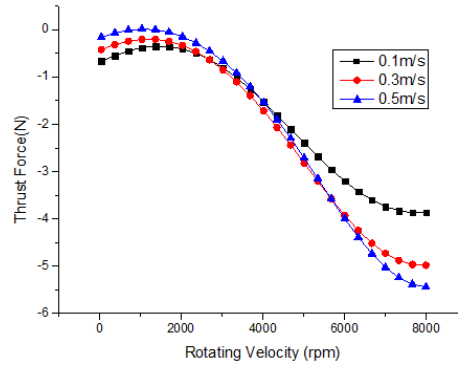

Fig.15 Relation of thrust force and rotating velocity

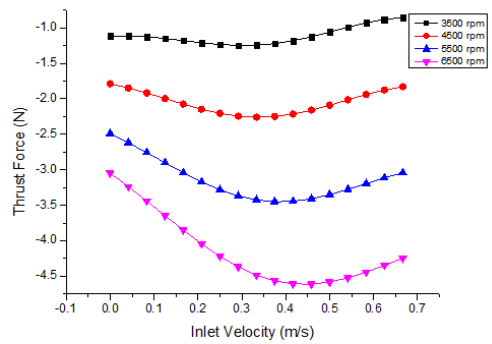

Fig.16 Relation of thrust force and inlet velocity

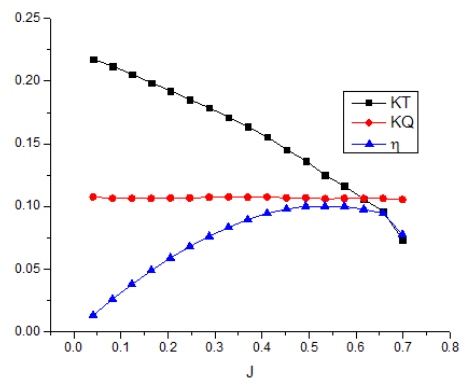

Fig.17 Characters of the novel thruster

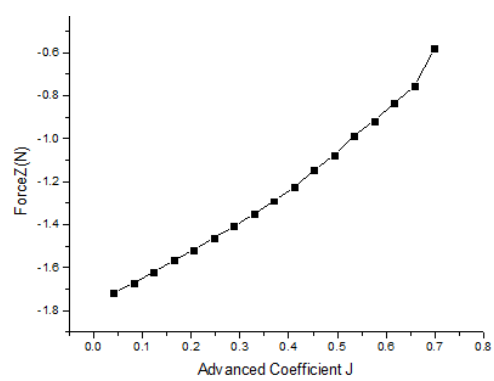

Fig.18 Thrust force with different J

ACKNOWLEDGMENT

This research is partly supported by the National High Tech. Research and Development Program of China (No.2015AA043202), National Natural Science Foundation of China (61773064, 61503028) and Graduate Technological Innovation Project of Beijing Institute of Technology (2018CX10022).

REFERENCES

[1] H. Xing, S. Guo, L. Shi, Y. He, S. Su, Z. Chen, and X. Hou, "Hybrid Locomotion Evaluation for a Novel Amphibious Spherical Robot," *Applied Sciences*, vol. 8, no. 2, pp. 156, 2018.

[2] AS Boxerbaum , P Werk, RD Quinn, and R Vaidyanathan, " Design of an autonomous amphibious robot for surf zone operation: part I mechanical design for multi-mode mobility," *IEEE International Conference on Advanced Intelligent Mechatronics*, pp.1459-1464, 2005.

[3] Crespi A, and Ijspeert A J, "AmphiBot II: An Amphibious Snake Robot that Crawls and Swims using a Central Pattern Generator," *Color Research & Application,* pp.130–135, 2006.

[4] Crespi, A.,Karakasiliotis, K., Guignard, A. and Ijspeert, A.J, "Salamandra Robotica II: An Amphibious Robot to Study Salamander-Like Swimming and Walking Gaits", *IEEE TRANSACTIONS ON ROBOTICS*, 29.2, pp:308-320, 2013.

[5] Yin X, Wang C, and Xie G, "A salamander-like amphibious robot: System and control design", *International Conference on Mechatronics and Automation. IEEE*, pp: 956-961, 2012.

[6] Yu J, Ding R, Yang Q, Tan M, Wang W, and zhang J, "On a Bio-inspired Amphibious Robot Capable of Multimodal Motion", *IEEE-ASME TRANSACTIONS ON MECHATRONICS*, 17(5), pp:847-856, 2012.

[7] Tang, Y. G., Zhang, A. Q., Jian cheng, Y. U., and Zhang, X. Q., "Multi-objective optimization design for the wheel-propeller-leg driving mechanism of an amphibious robot", *Robot*, 31(3), pp:276-280, 2009.

[8] Zhang, S.W, Zhou, Y.C, Xu, M, Liang, X, Liu, L, and Yang, J, "AmphiHex-I: Locomotory Performance in Amphibious Environments With Specially Designed Transformable Flipper Legs", *IEEE-ASME TRANSACTIONS ON MECHATRONICS*, 21.3, pp:1720-1731, 2016.

[9] Guo S, He Y, Shi L, Tang K, and Xiao R, "Modal and fatigue analysis of critical components of an amphibious spherical robot", *Microsystem Technologies*, 23(6), pp: 1-15, 2016.

[10] He, Y., Shi, L., Guo, S., Pan, S., and Wang, Z, "Preliminary mechanical analysis of an improved amphibious spherical father robot", *Microsystem Technologies*, 22(8), pp: 2051-2066, 2016.

[11] Guo, S., Pan, S., Shi, L., Guo, P., He, Y., and Tang, K., "Visual detection and tracking system for a spherical amphibious robot" *Sensors*, 17(4), pp: 870, 2017.

[12] Pan, S., Shi, L., and Guo, S, "A kinect-based real-time compressive tracking prototype system for amphibious spherical robots", *Sensors*, 15(4), pp: 8232-52, 2015.

[13] Li K, Yu J, Wu Z, and Tan. M, "Hydrodynamic analysis of a gliding robotic dolphin based on Computational Fluid Dynamics", *Control Conference. IEEE*, pp: 6008-6013, 2016.

[14] Guo S, He, Y, Shi, L, Pan, S, Xiao, R., and Tang, K, "Modeling and experimental evaluation of an improved amphibious robot with compact structure", *Robotics and Computer-Integrated Manufacturing*, 2018, 51, pp: 37-52, 2018.

[15] Guo, S., Pan, S., Li, X., Shi, L., Zhang, P., and Guo, P., "A system on chip-based real-time tracking system for amphibious spherical robots", *International Journal of Advanced Robotic Systems*, 14(4), pp: 1-19, 2017.

[16] Gu, S., and Guo, S, "Performance evaluation of a novel propulsion system for the spherical underwater robot (surIII)", *Applied Sciences*, 7(11), pp: 1196, 2017.

[17] Li, Y., Guo, S., and Wang, Y., "Design and characteristics evaluation of a novel spherical underwater robot", *Robotics & Autonomous Systems*, 94, pp: 61-74, 2017.

[18] Guo, J., Guo, S., and Li, L., "Design and characteristic evaluation of a novel amphibious spherical robot", *Microsystem Technologies*, 23(6), pp: 1999-2012, 2017.

[19] Li, Y., Guo, S., and Yue, C., "Preliminary concept of a novel spherical underwater robot", *International Journal of Mechatronics & Automation*, 5(1), 2015.

[20] Majdfar S, Ghassemi H, Forouzan H, and Ashrafi, A, "Hydrodynamic prediction of the ducted propeller by CFD solver", *Journal of Marine Science & Technology*, 25, 2017.

[21] Motallebi-Nejad, M., Bakhtiari, M., Ghassemi, H., and Fadavie, M., "Numerical analysis of ducted propeller and pumpjet propulsion system using periodic computational domain", *Journal of Marine Science & Technology* (3), pp: 1-15, 2017.

[22] Kim J, Han J, and Wan K C, "Accurate and Practical Thruster Modeling for Underwater Vehicles", *IEEE International Conference on Robotics and Automation. IEEE*, pp: 175-180, 2006.

[23] Ghassemi, H., Majdfar, S., and Forouzan, H, "Calculations of the hydrodynamic characteristics of a ducted propeller operating in oblique flow", *Ship Science and Technology*, 10(20), pp: 31, 2017.

[24] Wang, C., Sun, S., Sun, S., and Li, L, "Numerical analysis of propeller exciting force in oblique flow", *Journal of Marine Science & Technology*, (3), pp:1-18, 2017.